Desalination and Water Treatment
www.deswater.com

doi: 10.5004/dwt.2020.25866

201 (2020) 356–368
October

Preparation and characterization of hierarchical $BiOI_{0.5}Cl_{0.5}$ with excellent adsorption and photocatalytic abilities for removal of aquatic dyes

Yongli Zhang[a], Jian Zhang[a,b], Weihong Tang[a,c], Ningruo Wang[d], Yang Liu[a], Hongguang Guo[a,*]

[a]*College of Architecture and Environment, Sichuan University, Chengdu 610065, China, emails: hgguo@scu.edu.cn (H. Guo), zyl_scu@126.com (Y. Zhang), 409788551@qq.com (J. Zhang), 476273789@qq.com (W. Tang), 654458560@qq.com (N. Wang), 237668713@qq.com (Y. Liu)*
[b]*Chengdu Engineering Corporation Ltd., Power China, Chengdu 611130, China*
[c]*Chengdu Environmental Investment Group Co., Ltd., Chengdu 610065, China*
[d]*Institute for Disaster Management and Reconstruction Sichuan University-The Hong Kong Polytechnic University, Sichuan University, Chengdu 610065, China*

Received 11 October 2019; Accepted 20 March 2020

ABSTRACT

In this study, hierarchical bismuth oxyhalide $BiOI_{0.5}Cl_{0.5}$ was successfully synthesized and adopted for the adsorption and vis-photocatalytic removal of aquatic dyes. The morphology and physiochemical properties of $BiOI_{0.5}Cl_{0.5}$ were investigated by Fourier-transform infrared spectroscopy, UV-visible, diffuse reflectance spectroscopy, scanning electron microscopy, transmission electron microscopy, X-ray diffraction, Brunauer–Emmett–Teller. Three metachromatic dyes, Rhodamine B (RhB), Methylene blue (MB), and Congo red (CR)were selected as targets due to their photosensitivity. Several crucial factors concerning temperature, pH, material dosages, and scavengers were elucidated. The as-prepared $BiOI_{0.5}Cl_{0.5}$ exhibited sound adsorption capability for the three dyes, with the removal rate reaching 90.0%, 79.0%, and 83.2% for RhB, MB, and CR, respectively, after 120 min reaction, which could be well-fitted by the pseudo-second-order kinetics and the Langmuir model. Due to the promising performance of $BiOI_{0.5}Cl_{0.5}$, the removal of selected dyes was significantly enhanced under visible light irradiation. While the adsorption capacity of RhB and MB was decreased by 17.39% and 18.99%, respectively, the differential removal behaviors were observed in photocatalysis over the pH range of 2.0–10.0. The Langmuir–Hinshelwood (L–H) model for photochemical systems was established and verified for various conditions. Through scavenger study, the major reactive species for the degradation of the selected dyes using $BiOI_{0.5}Cl_{0.5}$ under visible light are h^+ and $^{\bullet}O^{2-}$ instead of $^{\bullet}OH$. This study provides potential insight into the removal of aquatic dyes using simultaneous adsorption and photochemical treatment under solar light.

Keywords: Bismuth oxyhalides; Organic dyes; Visible light; Adsorption; Photocatalysis; Kinetics

1. Introduction

Water pollution has become a global concern nowadays since many toxic pollutants are constantly finding their way into water resources [1,2]. Among the residual emerging organics in the environment, organic dyes, extensively used in printing, textile, and related biological industries, have been exhibiting high toxicity and potential carcinogenic effects, resulting in the deterioration of aquatic ecosystems by reducing the penetration of sunlight and oxygen [3,4]. Potential treatments have been adopted aiming at removing dyes from wastewater, such as adsorption [5], coagulation

* Corresponding author.

[6], biological treatment [7], membrane filtration [8], and oxidation [9]. Among these, adsorption and advanced oxidation processes have been demonstrated as the preferred technologies.

Owing to the photosensitivity of organic dyes, photocatalysis has been actively performed as an alternative method for dye-decontamination [10]. TiO_2 is usually adopted as a typical semi-conductive catalyst in the photocatalytic reactions due to its good performance and nontoxicity [11]. However, the large bandgap of TiO_2 (3.2 eV) restricts its potential use under visible light irradiation, as only a small UV fraction (about 2%–3%) of solar light can be utilized. Bismuth composites have been demonstrated to be promising materials for photodegradation under visible light irradiation, and research concerning $BiMO_4$ (M = V, W), $BiFeO_3$, and $Bi_{25}FeO_{40}$ has been conducted on organic pollutants degradation and water splitting due to their unique and excellent characteristics [12–15].

Recently, bismuth oxyhalides (BiOX, X = Cl, Br, and I) have been admitted as excellent adsorbents and photocatalysts for the removal of organic pollutants in water [16–20]. The band gaps of BiOX can be within 1.7–3.4 eV by varying the halides and the composition ratios of the two halides ($BiOX_\alpha Y_{1-\alpha}$) [21]. Owing to the high separation rate of photo-induced electron–hole pairs, the past 10 y have witnessed tremendous efforts in utilizing BiOCl as a promising catalyst for photocatalytic applications under visible light irradiation, including pollutants removal, N_2 fixation, CO_2 reduction, and water splitting [22, 23]. On the other hand, BiOI displays good efficiency in catalysis among BiOX materials due to its narrowest band gap and lower energy threshold [24]. Since the energy threshold and the separation/recombination rate of electron–hole pairs constitute the efficiency of visible light-driven reactions, materials synthesized by BiOCl, and BiOI have been widely adopted in the removal of organic dyes in water and air [17,25,26]. While most of the photocatalytic oxidation reactions based on BiOX usually need several hours or more for pollutants removal, and most of the studies mainly focused on single photocatalytic properties in organic pollutants decontamination, limited studies have been undertaken on simultaneous adsorption performance, resulting in inadequate investigations concerning the performance of metachromatic dyes in heterogeneous photocatalytic reactions. Therefore, further discussion combining integrated adsorption–photocatalysis system should be concerned and has potential possibility for textile dyes removal.

Hence, in the present study, we synthesized hierarchical $BiOI_{0.5}Cl_{0.5}$ using the solvothermal method, innovatively proposed a method that combined adsorption and photocatalysis to remove three organic metachromatic dyes: Rhodamine B, Methylene blue, and Congo red, which are commonly used in the chemical and textile industries. Multiple characterizations including Fourier-transform infrared spectroscopy (FTIR), X-ray diffraction (XRD), scanning electron microscopy (SEM), transmission electron microscopy (TEM), Brunauer–Emmett–Teller (BET) and UV-visible (UV-vis) were applied to evaluate the physicochemical performance of $BiOI_{0.5}Cl_{0.5}$. The application of $BiOI_{0.5}Cl_{0.5}$ in dye-adsorption was investigated in regard to the adsorption kinetics, isotherms and the pH effect. Furthermore, the photocatalytic degradation of the three dyes in aqueous solution by $BiOI_{0.5}Cl_{0.5}$ were evaluated under simulated solar irradiation, and crucial factors including the effect of catalyst loading, pH variation, and the active species identification were elucidated. The related kinetic model, including the simultaneous adsorption and photocatalysis was established and tested with the catalytic mechanism proposed for the photocatalytic process.

2. Material and methods

2.1. Chemicals

$Bi(NO_3)_3{\cdot}5H_2O$, KI, KCl, Rhodamine B, Methylene blue, and Congo red were purchased from Kelong Chemical Reagent Co., (Chengdu, China). All other chemical reagents were analytical grade and used without further purification. The typical solutions used were prepared using Milli-Q water system (18.2 M Ωcm^{-1}).

2.2. Synthesis of $BiOI_{0.5}Cl_{0.5}$, BiOI, and BiOCl

The $BiOI_{0.5}Cl_{0.5}$ was synthesized in the modified procedure reported in previous studies [17]. Briefly, 8.731 g $Bi(NO_3)_3{\cdot}5H_2O$ was dissolved in 180 mL ethylene glycol under intense stirring for 30 min to obtain solution A. Then, 1.494 g KI and 0.672 g KCl was dissolved in 180 mL water to obtain solution B, respectively. Afterwards, solution B was added rapidly into the solution A under intense stirring for 2 h at the ambient temperature. The resulting mixture was calcined at 180°C for 24 h in a stainless-steel autoclave equipped with a teflon lining. Finally, the products $BiOI_{0.5}Cl_{0.5}$ was separated and washed three times with ethanol and water, then dried at 60°C, in a vacuum drying oven until use. For comparison, the BiOI and BiOCl was synthesized with the same procedure, using 2.989 g KI (for BiOI) and 1.344 g KCl (for BiOCl).

2.3. Characterization

Concentrations of Rhodamine B, Methylene blue, and Congo red were measured at 554, 664, and 488 nm, respectively, with a UV-vis spectrophotometer (MAPADA, UV-1800PC, China). The crystal structural characterization of $BiOI_{0.5}Cl_{0.5}$ was conducted by powder XRD spectrometry using an Empyrean diffractometer advance instrument between 10° and 80° (2θ) (PANalytical B.V, Holland). To determine the morphology of the as-prepared samples, SEM measurements were run using a JSM-7500F (JEOL, Japan) at 20 kV. A JW-BK122F specific surface area analyzer (JWGB, China) was adopted to measure the specific surface area and pore distribution of the catalysts using the nitrogen adsorption–desorption with BET analysis. The FTIR spectrometer results were obtained using a Nicolet iS10 FTIR spectrometer (Thermo Scientifc, United States), in the range of 400–4,000 cm^{-1} wavenumbers. By using the UV-vis spectrophotometer (MAPADA, UV-1800PC, China), the UV-vis diffuse reflection spectra (DRS) for the samples were obtained.

Since mg L^{-1} level concentration of dyes are diffusely emerging in wastewater outlets, relatively higher concentrations were adopted for the selected targets to exhibit the excellent performance for the adsorption and photocatalytic process, in order to make the initial concentration of

the three dyes in the precise detection range of the UV-vis spectrophotometer. In a typical adsorption experiment, 0.025 g of prepared sample was added to a 50 mL of solution containing 10 mg L^{-1} Rhodamine B, Methylene blue, and 80 mg L^{-1} Congo red, respectively. The experiments were carried out in an orbit shaker with continuous mixing at 200 rpm in a temperature-controlled environment. Afterwards, a 4.0 mL sample was withdrawn and filtrated using a 0.22 μm filter before concentration detection.

The photocatalytic activities of the synthesized samples were evaluated for the degradation of Rhodamine B, Methylene blue, and Congo red solutions under visible light irrigation at ambient temperature. Typical experiments were carried out in a double-walled reactor (diameter 14.0 cm, height 10.0 cm) with water bath. A 500 W Xenon lamp with a 420 nm cutoff filter was adopted as the light source, which was positioned 30 cm above the glass reactor to trigger the photocatalytic reaction. The light intensity was controlled and all the suspensions were magnetically stirred for 5 min in the dark before the irradiation, in order to compare the degradation effect between adsorption and photocatalysis. The solution pH was adjusted using 0.1 M NaOH and HCl to the regulated value when it was needed. Triplicate tests were conducted and the average values with the standard deviations are presented.

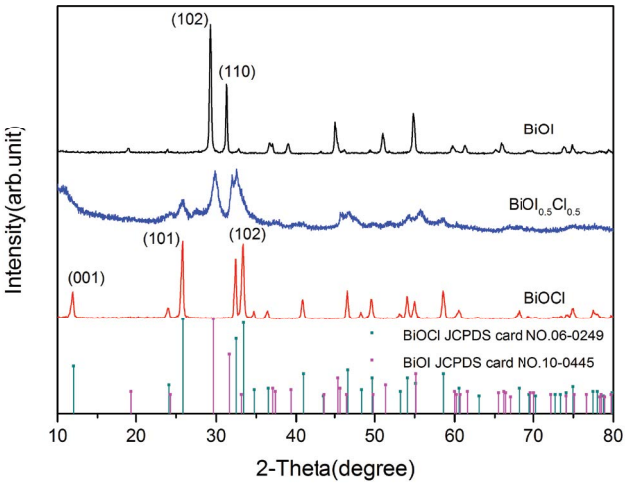

Fig. 1. XRD patterns of BiOI, BiOCl, and $BiOI_{0.5}Cl_{0.5}$.

3. Results and discussion

3.1. Characterization of the synthesized samples

XRD was applied to characterize the chemical composition and crystalline structure of the synthesized $BiOI_{0.5}Cl_{0.5}$. The patterns of the samples are presented in Fig. 1. It is clearly shown that BiOX can be indexed to the tetragonal phase structure BiOI (JCPDS card NO.10–0445) and BiOCl (JCPDS card NO.06–0249), indicating a high purity of the products. Moreover, the XRD peaks of the $BiOI_{0.5}Cl_{0.5}$ sample is weaker and broader than the pure BiOI and BiOCl, demonstrating a smaller particle size and lower crystallinity to a certain extent [27]. The major peaks are positioned at $2\theta = 11.1°$, 25.8°, 29.9°, 32.0°, and 32.6°. The shift of the (001), (101), (102), and (110) planes are strong evidence in determining the intercalated layer products [28].

Fig. 2 shows the SEM and TEM images of the synthesized $BiOI_{0.5}Cl_{0.5}$. Clearly, the prepared $BiOI_{0.5}Cl_{0.5}$ is dominated with the hierarchical nanoplates [28]. The size of $BiOI_{0.5}Cl_{0.5}$ spreads from 100 to 200 nm. The image reveals the nanoplates of the samples with ordered lattice fringes and interplanar spaces. The formation of a 2-dimension nanoplates structure can be ascribed to the internal structure of $BiOI_{0.5}Cl_{0.5}$, where the $[Bi_2O_2]^{2+}$ layers are interleaved by two slabs of X^- atoms, leading to the anisotropic growth at a certain axis [29].

The nitrogen adsorption–desorption test was conducted using the BET method, with the results presented in Fig. 3. The inset shows the BJH pore size distribution for the prepared samples. $BiOI_{0.5}Cl_{0.5}$ has a large surface area (44.94 m^2 g^{-1}) and pore volume (0.454 cm^3 g^{-1}), which is consistent with the results of SEM. Fig. 3 identifies the as-prepared sample as type V with an H3 hysteresis loop, suggesting mesoporous features [30]. It is demonstrated that a greater specific

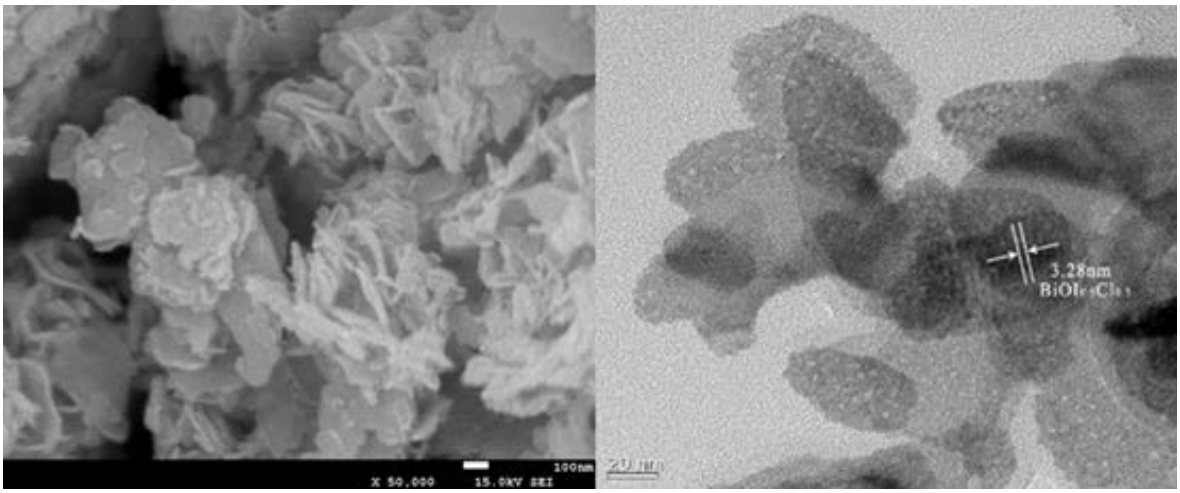

Fig. 2. SEM and TEM images of $BiOI_{0.5}Cl_{0.5}$.

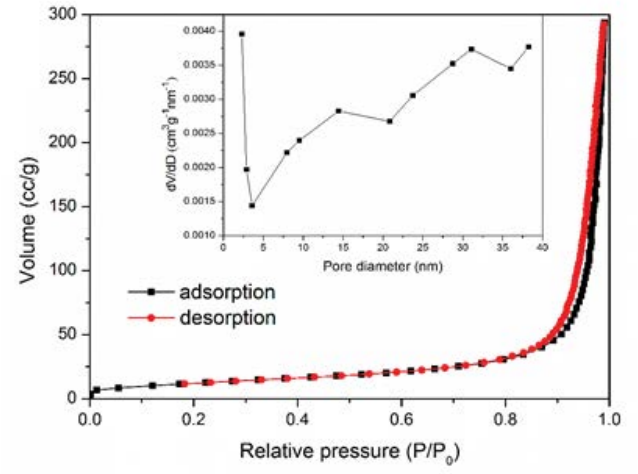

Fig. 3. Nitrogen adsorption–desorption isotherms of $BiOI_{0.5}Cl_{0.5}$.

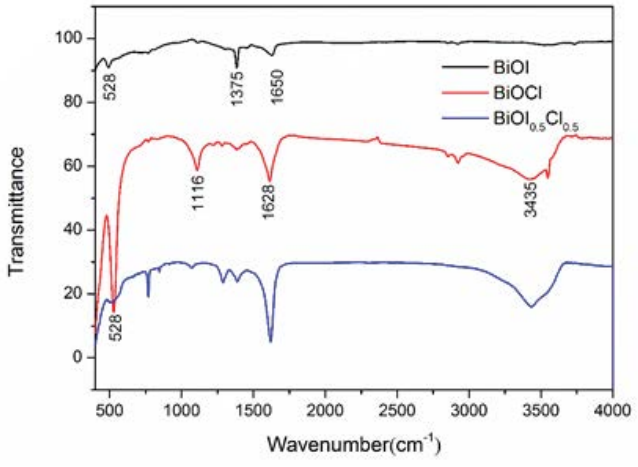

Fig. 5. FTIR spectra of synthesized $BiOI_{0.5}Cl_{0.5}$, BiOI, and BiOCl.

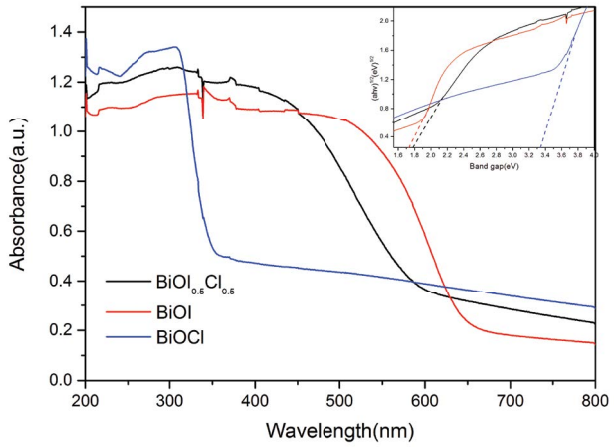

Fig. 4. UV-vis diffuse reflectance spectra and band gaps (E_g) of as-prepared samples.

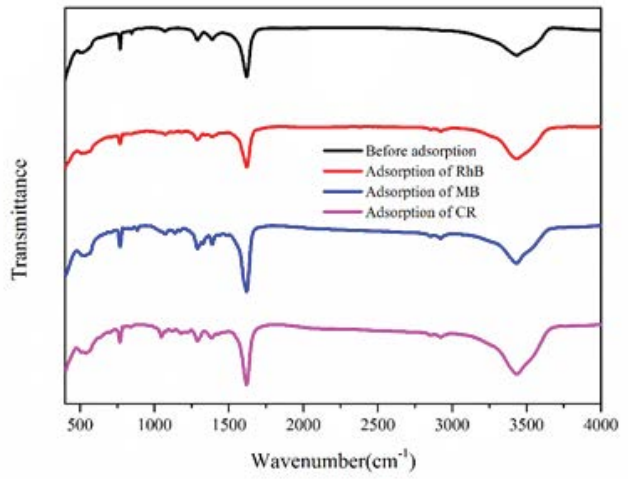

Fig. 6. FTIR spectra of the as-prepared $BiOI_{0.5}Cl_{0.5}$ before and after adsorption of the three dyes.

surface area and pore volume of photocatalysts can favor the sorption of substrates and supply a higher surface density of the active sites, leading to an enhancement of the adsorption and photocatalytic performance [27].

The optical property is an important indicator for semiconductor photocatalysts. In order to compare the relevant photacatalytic performance, the UV-vis–DRS of the as-prepared BiOI, BiOCl, and $BiOI_{0.5}Cl_{0.5}$ is presented in Fig. 4. As can be seen, all the three materials have responses to the visible light. For a crystalline semiconductor, the optical absorption near the band edge follows Eq. (1) [31]:

$$\alpha h\upsilon = A\left(h\upsilon - E_g\right)^{1/2} \quad (1)$$

where α is the adsorption coefficient, A is a constant, hυ stands for the photon energy, and E_g is the band gap energy. In this study, the band gaps of BiOI, BiOCl, and $BiOI_{0.5}Cl_{0.5}$ are obtained as 1.73, 3.33, and 1.78 eV, respectively, from the intercept of the tangents to the plots [32]. It can be seen that $BiOI_{0.5}Cl_{0.5}$ shows a relatively smaller E_g than BiOCl and close similarity to BiOI, demonstrating superior photocatalytic property under visible light irradiation.

FTIR spectra was applied to investigate and compare the functional groups on BiOI, BiOCl, and $BiOI_{0.5}Cl_{0.5}$. As shown in Fig. 5, characteristic absorption peaks at 528; 1,375; and 1,650 cm^{-1} are observed in BiOI. The peak at 528 cm^{-1} is associated with the Bi–O stretching mode, while the absorption peaks at 1,375 and 1,650 cm^{-1} could be assigned as the asymmetry and symmetric stretching vibration peaks for Bi–I band [33]. Similar characteristic peaks emerge at 1,116 and 1,628 cm^{-1} for the Bi–Cl band in the BiOCl structure. The band at 3,435 cm^{-1} for $BiOI_{0.5}Cl_{0.5}$ and BiOCl is the stretching and flexural vibration of O–H in the free water, and the same characteristic peaks at 1,375 and 1,650 cm^{-1} demonstrate the coexistence of BiOI [34]. Besides, no insignificant change is observed between the fresh and used adsorbent illustrated in Fig. 6, indicating the physical adsorption of $BiOI_{0.5}Cl_{0.5}$.

3.2. Adsorption performance

3.2.1. Surface adsorption kinetics

The adsorption kinetic results are illustrated in Fig. 7a. $BiOI_{0.5}Cl_{0.5}$ shows high adsorption capacities for the three dyes, with the removal rate reaching 90.0%, 79.0%, and 83.2% for RhB, MB, and CR, respectively, after 120 min contact. The adsorption process can be divided into a quick step and a stable step. Rapid removal was observed during the first 10 min due to the large amounts of available adsorption sites on the surface of $BiOI_{0.5}Cl_{0.5}$ and the higher concentration gradient of the adsorbates. It has been demonstrated that strong interactions between the adsorbate and adsorbent gave rise to a higher adsorption efficiency in a short time [35]. Afterwards, the adsorption sites are gradually saturated, with removal efficiency remaining stable until equilibrium.

Pseudo-second-order models expressed in Eq. (2) were adopted to illustrate the kinetics for the adsorption of the three dyes using $BiOI_{0.5}Cl_{0.5}$:

$$\frac{t}{Q_t} = \left(kQ_e^2\right)^{-1} + \frac{t}{Q_e} \tag{2}$$

where Q_t is the adsorption capacity at time t (mg g^{-1}); Q_e is the adsorption capacity at equilibrium (mg g^{-1}); k is the rate parameters of the pseudo-second-order.

As summarized in Table 1, the results indicate that the adsorption fits excellently to the pseudo-second-order kinetics model with Q_e obtained as 17.86, 15.27, and 138.89 mg g^{-1} for RhB, MB, and CR, respectively (shown in the inset of Fig. 7a).

3.2.2. Effect of initial pH

Since most of the metachromatic dyes exhibit different properties and spectroscopy with pH variation, the influence of the initial pH on the adsorption was investigated. As an acidic indicator, Congo red can get sharp color transition under acidic conditions, hence, pH 8.0, 10.0, and 12.0 were selected as evaluated conditions, while the entire pH range was adopted for Rhodamine B and Methylene blue. As shown in Fig. 8, with pH increased from 2.0 to 10.0, the adsorption capacity for RhB and MB was decreased by 17.39% and 18.99%, respectively, while a stable adsorption performance (maximum adsorption capacity of 139.5 mg g^{-1} at pH 10.0) was obtained for CR. It can be explained by the isoelectric point of $BiOI_{0.5}Cl_{0.5}$ and the protonated/deprotonated properties of the selected dyes.

Table 1
Kinetic parameters using pseudo-second-order model for adsorption of the three dyes on $BiOI_{0.5}Cl_{0.5}$

Dyes	C_0 (mg L^{-1})	k	Q_e (mg g^{-1})
RhB	10	0.0166	17.86
MB	10	0.0218	15.27
CR	80	0.00095	138.89

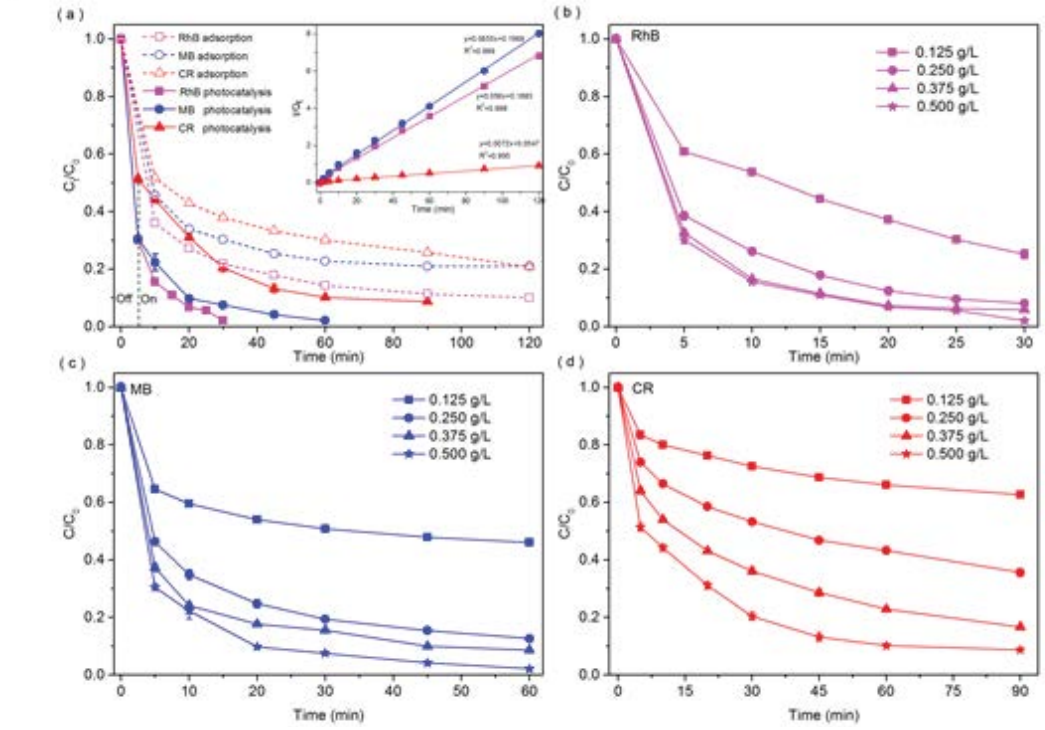

Fig. 7. (a) Photocatalytic and adsorption capacities for three dyes using $BiOI_{0.5}Cl_{0.5}$ (inset: adsorption fitted by the pseudo-second-order kinetic model). Effect of catalyst dosages on the photocatalytic degradation of (b) RhB dye, (c) MB dye, and (d) CR dye (catalyst dosage = 0.500 g L^{-1}, RhB = 10 mg L^{-1}, MB = 10 mg L^{-1}, CR = 80 mg L^{-1}).

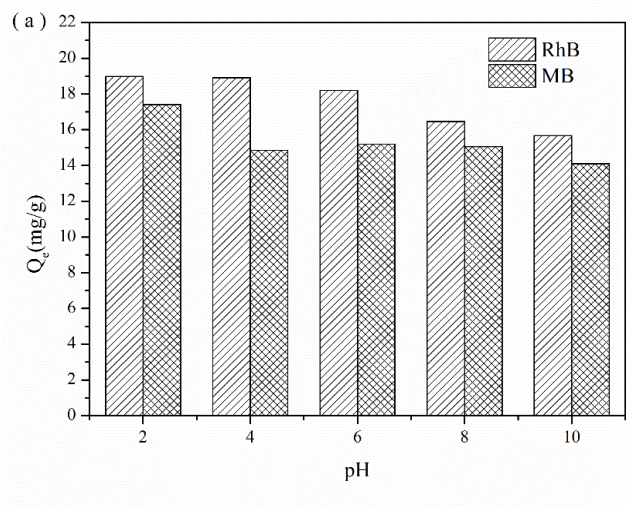

Fig. 8. Effect of pH on the adsorption of RhB, MB (a), and CR (b) by $BiOI_{0.5}Cl_{0.5}$ ([dosage] = 0.500 g L^{-1}; RhB and MB dyes = 10 mg L^{-1}, CR dye = 80 mg L^{-1}, T = 303 K).

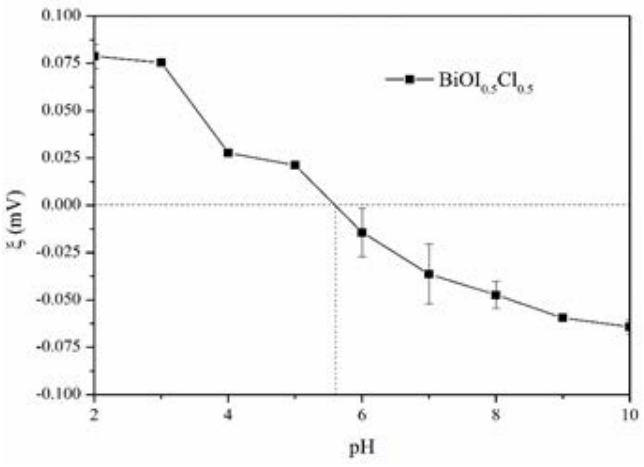

Fig. 9. Zeta potential vs. pH for the as-prepared $BiOI_{0.5}Cl_{0.5}$.

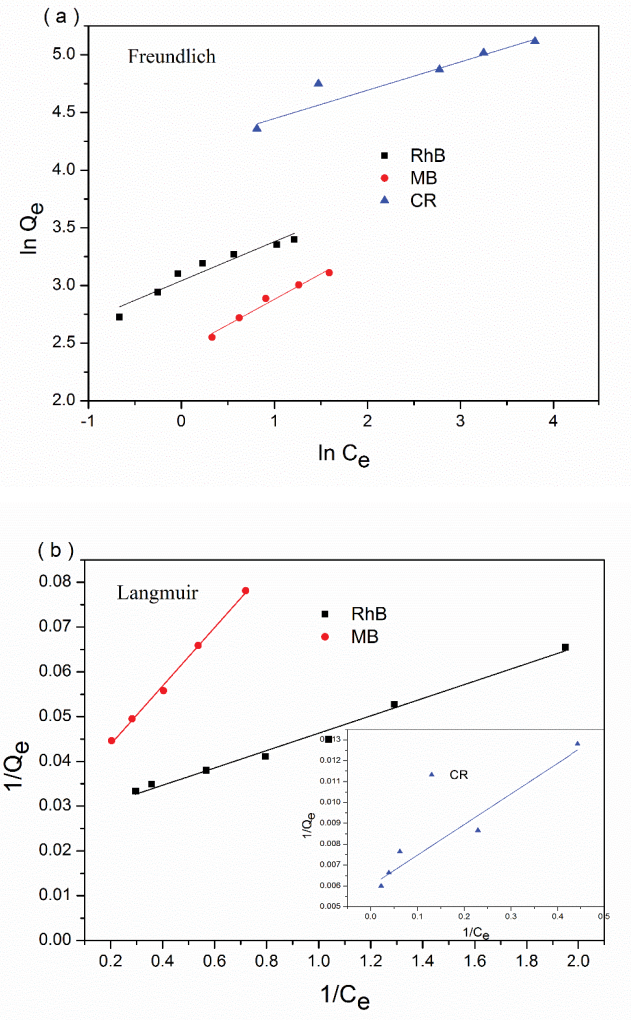

Fig. 10. Adsorption isotherm for the three dyes using $BiOI_{0.5}Cl_{0.5}$ fitted by Freundlich (a) and Langmuir model (b) (catalyst dosage = 0.500 g L^{-1}, RhB = 10 mg L^{-1}, MB = 10 mg L^{-1}, CR = 80 mg L^{-1}, T = 303 K).

According to a previous study, the pKas value of RhB, MB, and CR are, respectively, 3.2, 3.8, and 4.1 [36–38], while in this study, the isoelectric point of $BiOI_{0.5}Cl_{0.5}$ is obtained as 5.6 V (illustrated in Fig. 9 through Zeta potential detection) [39]. It is deduced that when the pH is below 5.6, the synthesized $BiOI_{0.5}Cl_{0.5}$ is positively charged. Due to the electrostatic characterization of RhB in various pH conditions, the maximum adsorption capacity is observed at pH 4.0, which is quite different with MB and CR. For MB, protons tend to compete for the adsorption sites on the functional groups of $BiOI_{0.5}Cl_{0.5}$ at lower pH, while the positively charged surface ligands decreased with the pH increasing, reducing the interaction between the adsorbing material and the targets. Since CR and $BiOI_{0.5}Cl_{0.5}$ remained negatively charged from pH 8.0 to 12.0, the adsorption capacity for CR was basically unstable with little variation observed.

Table 2
Fitting parameters of Freundlich and Langmuir models for three dyes

Dyes	Kinetic models	Parameters
RhB	Freundlich	$y = 0.3391x + 3.0406$, $R^2 = 0.9299$, $n = 2.95$, $K_F = 20.92$
	Langmuir	$y = 0.0194x + 0.0269$, $R^2 = 0.9886$, $q_0 = 37.17$, $K_L = 1.39$
MB	Freundlich	$y = 0.4417x + 2.4382$, $R^2 = 0.9774$, $n = 2.26$, $K_F = 11.45$
	Langmuir	$y = 0.0652x + 0.0308$, $R^2 = 0.9968$, $q_0 = 32.47$, $K_L = 0.47$
CR	Freundlich	$y = 0.2257x + 4.276$, $R^2 = 0.9105$, $n = 4.43$, $K_F = 71.95$
	Langmuir	$y = 0.0147x + 0.006$, $R^2 = 0.9577$, $q_0 = 166.67$, $K_L = 0.41$

3.2.3. Surface adsorption isotherms

The results of the isotherms models for the removal of the selected dyes using the synthesized $BiOI_{0.5}Cl_{0.5}$ are evaluated with several experiments. 0.025 g $BiOI_{0.5}Cl_{0.5}$ were added to 50 mL solution containing different concentrations of dyes were performed to evaluate Freundlich and Langmuir adsorption models, calculated by following equations (Eqs. (3)–(4)), respectively, and shown in Fig. 10, with the fitting results summarized in Table 2. Compared to the Freundlich model, the adsorption of the three dyes are preferably fitted by the Langmuir model with a higher correlation coefficient, suggesting that the monolayer sorption on the surface of $BiOI_{0.5}Cl_{0.5}$ is more pronounced.

$$\ln Q_e = \ln K_F + \frac{1}{n}\ln C_e \tag{3}$$

$$\frac{1}{Q_e} = \frac{1}{K_L Q_0}\cdot\frac{1}{C_e} + \frac{1}{Q_0} \tag{4}$$

where K_F and n^{-1} is the Freundlich constants corresponding to adsorption capacity and intensity, respectively, C_e (mg L^{-1}) and Q_e (mg g^{-1}) are the equilibrium concentration and the amount of dyes adsorbed, respectively, Q_0 is the maximum adsorption capacity in theory; K_L is the Langmuir constant responding to adsorption energy.

3.2.4. Adsorption thermodynamics

To evaluate the thermodynamics for the adsorption of the organic pollutants, relevant experiments at 303, 313, and 323 K were conducted. The results reveal that increasing temperature showed promotion of the adsorption capacity of MB and CR, while insignificant variation was observed for RhB as shown in Fig. 11. Based on the results obtained, the thermodynamic parameters were evaluated for each compound by the following equations with $\Delta H°$, $\Delta S°$, and $\Delta G°$ summarized in Table 3:

$$\ln K_d = \frac{\Delta S°}{R} - \frac{\Delta H°}{RT} \tag{5}$$

$$\Delta G° = \Delta H° - T\Delta S° \tag{6}$$

In our study, the $\Delta G°$ values calculated for the three dyes adsorption are all negative, indicating the spontaneous and feasible process in water treatment. For MB and CR, the positive $\Delta H°$ and $\Delta S°$ values confirmed the endothermic nature for the adsorption process and the increasing randomness at the solid-solution interface. However, for RhB, the negative $\Delta H°$ indicated that the adsorption was an exothermic reaction. Since the $\Delta G°$ value was basically unchanged in the temperature range 303–323 K, it is deduced that the temperature influence on the adsorption experiment is limited, which is in accordance with previous studies concerning dye-adsorption [5].

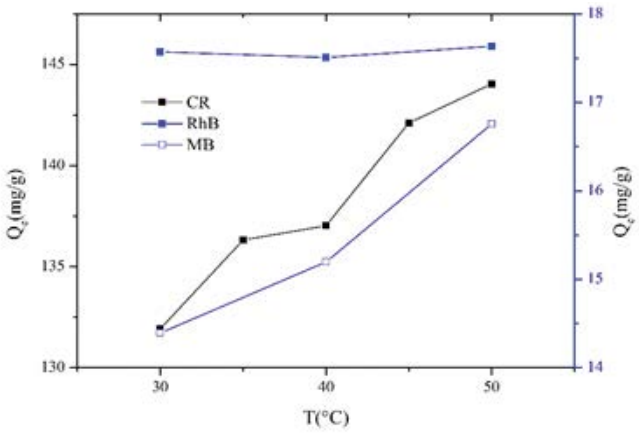

Fig. 11. Effect of the reaction temperature on the adsorption of the selected dyes using $BiOI_{0.5}Cl_{0.5}$ (catalyst dosage = 0.500 g L^{-1}, RhB = 10 mg L^{-1}, MB = 10 mg L^{-1}, CR = 80 mg L^{-1}, T = 303 K).

3.3. Photocatalytic degradation of the three dyes under simulated visible light

To evaluate the photocatalytic performance of $BiOI_{0.5}Cl_{0.5}$, the degradation of the three dyes under simulated visible light irradiation ($\lambda > 420$ nm) is displayed in Fig. 7. Since the most significant adsorption was observed in the initial stage, all the suspensions were magnetically stirred for 5 min in the dark before the irradiation. Compared to the adsorption process in Fig. 7a, the removal efficiency is obviously enhanced in the coupled system. RhB, MB, and CR were photodegraded completely in 30, 60, and 90 min, respectively.

Photocatalysis using semiconductors mainly relies on the excitation transition of electrons after illumination to form a highly active electron–hole pair, which can react with the OH^- and H_2O adsorbed on the surface of the semiconductor, leading to the free radicals formation. Besides, the degradation performance of selected dyes is also effected by

the generation of active species and surface transfer of the charge carriers, which are cooperatively determined by the electronic structure and surface properties [40]. In the morphology analysis of the obtained samples above (Fig. 2), the presence of thin nanoplates could contribute to the excellent photocatalytic performance, attributed to the high light utilization efficiency [41].

3.4. Effect of catalyst loading in photocatalytic degradation

In this section, various dosages of $BiOI_{0.5}Cl_{0.5}$ at 0.025, 0.050, 0.075, and 0.100 g were used for the degradation of the organic dyes. As shown in Figs. 7b–d, the rate of degradation was obviously enhanced with the increasing catalyst amounts due to the more active sites on the composites [42]. It has been demonstrated by previous studies that an optimal dosage exists in heterogeneously photocatalytic reactions, which can be attributed to the light scattering of the catalyst, however, in this study, a similar phenomenon was not observed [43].

3.5. Effect of pH in photocatalytic degradation

It was demonstrated that pH can affect the photocatalytic degradation concerning the concentration and reactive oxygen species (ROS). Previous studies have reported that the degradation of RhB decreased with increasing pH when using BiOI as a photo catalyst, due to the scavenging effect of hydroxyl radicals by H^+ [42]. Compared with BiOI and BiOCl, the prepared $BiOI_{0.5}Cl_{0.5}$ has a lower hydrogen evolution rate from the deionized water. In this study, the pH effects on the degradation of selected dyes using $BiOI_{0.5}Cl_{0.5}$ were evaluated, and the results are shown in Fig. 12. It is observed that the removal efficiency of the selected dyes exhibits particular performance in the range of pH 2.0–10.0. RhB degradation is independent of pH, while inhibition was obtained for MB, and slightly promotion was observed in the photocatalytic removal of CR. This could be attributed to the systematic impact caused by the deprotonation-protonation ratio for the selected organics, the surface charge of $BiOI_{0.5}Cl_{0.5}$ and the ROS, regarding the pH variation [44]. The synthetic effect could vary for the characteristics of selected dyes adsorbed on the surface of the catalyst as well as the photocatalytic preference in the bulk solution. Differing from the decrease in single adsorption, the pH independence of RhB under visible light irradiation indicates that the introduction of the vis-light photons has a crucial influence on the reactions [45]. It is demonstrated that increasing pH could promote ROS generation through vis-light photocatalytic degradation, which can play a supplementary role for RhB removal [46]. The removal rate of MB decreased with the pH increasing from 2.0 to 10.0, which was in accord with the adsorption process. As discussed in the previous section, both MB and the surface of $BiOI_{0.5}Cl_{0.5}$ were protonated with a positive charge when the pH is below 4.0, while the deprotonation of MB emerged in the range of 4.0–6.0, leading to the optimal removal rate of MB due to the preferred electrostatic attraction and following radical reactions between MB and $BiOI_{0.5}Cl_{0.5}$ [47]. Of note, the photochemical degradation of CR shows a slight promotion with the pH increasing from 8.0 to10.0, indicating that the emerging ROS in the bulk solutions play an efficient role compared to the single adsorption of CR. The results demonstrate that the $BiOI_{0.5}Cl_{0.5}$ maintained a good stability for photocatalytic performance under various pH conditions.

Table 3
Adsorption thermodynamics parameters of the three dyes on $BiOI_{0.5}Cl_{0.5}$

Dyes	T (K)	$\Delta G°$ (KJ mol^{-1})	$\Delta H°$ (KJ mol^{-1})	$\Delta S°$ (J mol^{-1} K^{-1})
RhB	303	–5.49	–6.64	–3.80
	313	–5.45		
	323	–5.41		
MB	303	–2.71	30.76	110.47
	313	–3.82		
	323	–4.92		
CR	303	–3.52	20.18	78.22
	313	–4.30		
	323	–5.09		

3.6. Recyclability of catalyst to degrade the three dyes

In order to evaluate the reusability of $BiOI_{0.5}Cl_{0.5}$ sample, the catalyst was collected by filtration from aqueous solution,

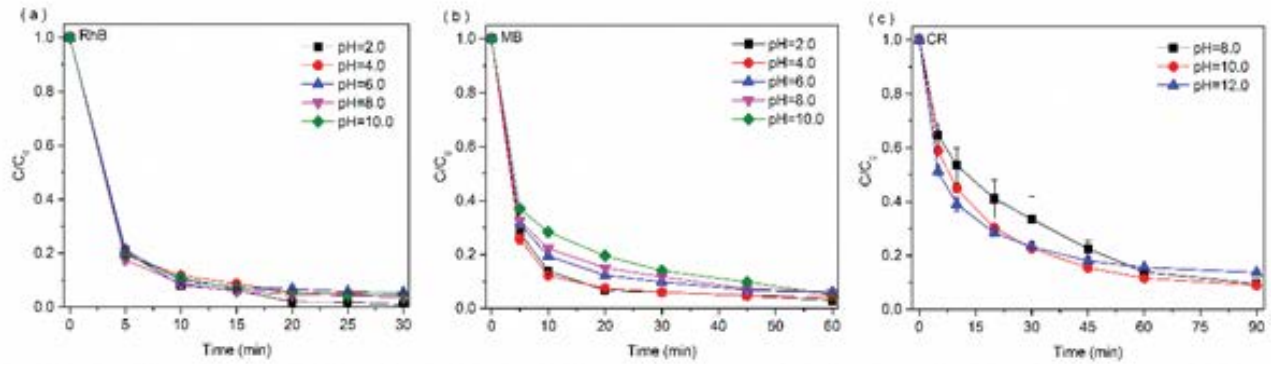

Fig. 12. Effect of pH on the photocatalytic degradation of (a) RhB dye (10 mg L^{-1}), (b) MB dye (10 mg L^{-1}), and (c) CR dye (80 mg L^{-1}, catalyst dosage = 0.500 g L^{-1}, RhB = 10 mg L^{-1}, MB = 10 mg L^{-1}, CR = 80 mg L^{-1}).

washed by ethanol and ultrapure water, then reused for degradation tests. Fig. 13 shows four recycling runs of the three dyes degradation, it was noticeable that the regeneration efficiency (defined as $(1–C_t/C_0)$) remained about 80% even after four cycles. The removal of RhB, MB, and CR were decreased 16.91%, 14.61%, and 14.41%, respectively. This activity decrease in the regeneration efficiency is possible due to the remarkable amounts of both dye molecules and by-products are adsorbed on the surface of catalyst, then the catalytic surface activity and the rate of mineralization are limited [48]. Overall, the $BiOI_{0.5}Cl_{0.5}$ catalyst showed good stability and potential for repeated use.

3.7. Kinetic analysis

According to the previous studies, the Langmuir–Hinshelwood (L–H) kinetics model has been widely used to describe the heterogeneous catalytic oxidation of dissolved organic compounds, and is expressed as below [49]:

$$-\frac{dC}{dt}=\frac{kKC}{1+KC} \tag{7}$$

where C is the concentration for the organic dyes, K is the equilibrium constant for the adsorption, and k is the rate constant.

In our study, Eq. (7) could be modified to Eq. (8) based on the studies of Asenjo et al. [49] and Li and Chen [50]:

$$C^{1-n}=(n-1)k_{app}+C_0^{1-n} \tag{8}$$

where C_0 (mmol L^{-1}) is the initial concentration of the organics, k_{app} is the apparent rate constant for the system, and n represents the order of the reaction.

The fitting results for the kinetic analysis of the dye-degradation are illustrated in Fig. 14, with the k_{app} and n values summarized in Table 4 under the various conditions. The correlation coefficients of R^2 indicate that Eq. (8) can well-simulate the degradation of the three organic dyes. It is deduced that the fitting results concerning catalyst dosage and pH are in accordance with the results obtained in the previous section.

3.8. Active species generated in the photocatalytic process and photocatalytic mechanism. of $BiOI_{0.5}Cl_{0.5}$

Previous studies have demonstrated that several ROS would exist in the photocatalytic reactions including the superoxide radical ($^{\bullet}O_2^-$), holes (h^+), electrons (e^-), hydroxyl radicals ($^{\bullet}OH$), and single oxygen ($^1O_2$). Hence, various

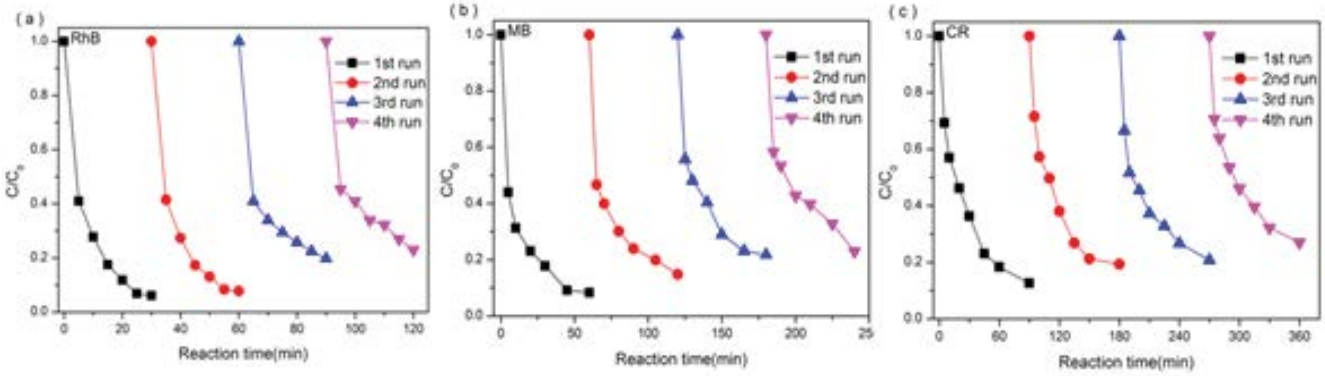

Fig. 13. Reusability of the $BiOI_{0.5}Cl_{0.5}$ samples to degrade (a) RhB dye (10 mg L^{-1}), (b) MB dye (10 mg L^{-1}), and (c) CR dye (80 mg L^{-1}, catalyst dosage = 0.500 g L^{-1}, RhB = 10 mg L^{-1}, MB = 10 mg L^{-1}, CR = 80 mg L^{-1}).

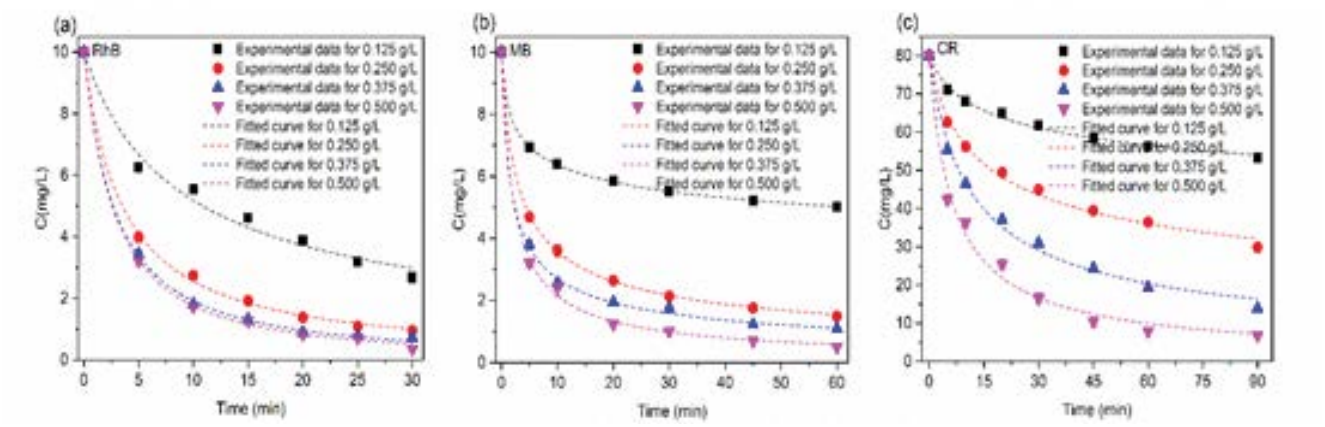

Fig. 14. Fitting performance using L–H model on effect of catalyst dosages for degradation of (a) RhB, (b) MB, and (c) CR (RhB = 10 mg L^{-1}, MB = 10 mg L^{-1}, CR = 80 mg L^{-1}, T = 303 K).

Table 4
Fitting parameters for the selected organic compounds degradation using Langmuir–Hinshelwood model under various conditions

Dyes	Initial pH	Dosage (g L^{-1})	n	k_{app} (mg^{1-n} L^{n}-1 min^{-1})	R^2
RhB	5.2	0.125	1.778	0.01247	0.9863
	5.2	0.250	1.815	0.037	0.9971
	5.2	0.375	1.8017	0.0545	0.9994
	5.2	0.500	1.367	0.0886	0.9627
MB	6.3	0.125	6.6613	2.38E-6	0.9995
	6.3	0.250	2.863	0.004074	0.9996
	6.3	0.375	2.756	0.008054	0.9827
	6.3	0.500	1.8873	0.0353	0.9992
CR	6.9	0.125	4.609	1.55E-08	0.9273
	6.9	0.250	3.248	2.08E-06	0.9912
	6.9	0.375	2.079	0.000502	0.9959
	6.9	0.500	2.089	0.001308	0.9740

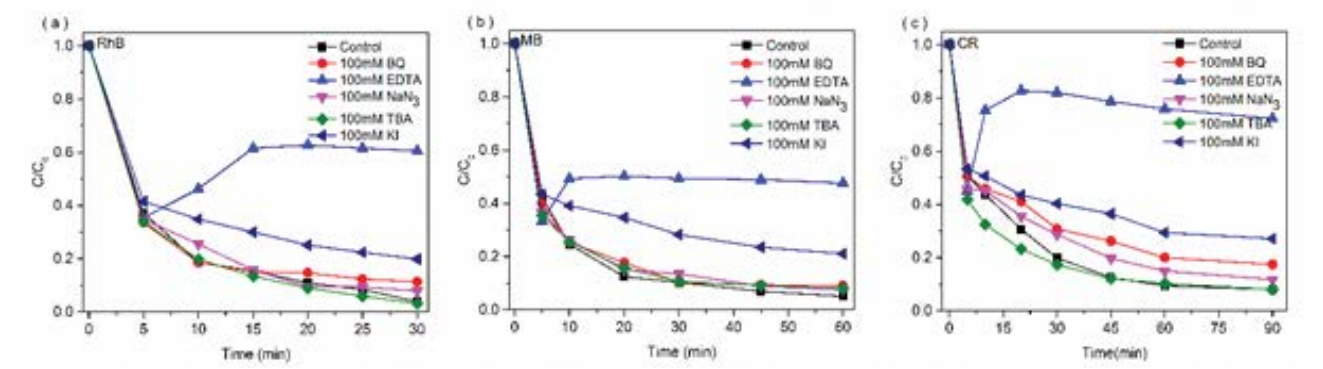

Fig. 15. Scavenging effects on removal of the three organic dyes by the Vis/$BiOI_{0.5}Cl_{0.5}$ systems (catalyst dosage = 0.500 g L^{-1}; [scavenger] = 100 mM; (a) RhB = 10 mg L^{-1}, pH = 5.2; (b) MB = 10 mg L^{-1}, pH = 6.3; (c) CR = 80 mg L^{-1}, pH = 6.9).

targeted quenchers were selected and adopted to identify the ROS in our system. In this section, 100 mM *p*-benzoquinone (BQ, a quencher of $^{\bullet}O_2^-$), EDTA(a quencher of h^+), sodium azide (NaN_3, a quencher of $^1O_2$, $k = 1 \times 10^9$ M^{-1} s^{-1}), *t*-butyl alcohol (TBA, a quencher of $^{\bullet}OH$, $k = 6 \times 10^8$ M^{-1} s^{-1}) and potassium iodide (KI, a quencher of e^-) were used in the decontamination of the selected dyes [51–55]. As shown in Fig. 15, when NaN_3 and TBA were added, insignificant inhibition was observed, and limited inhibition emerges for BQ quenching especially for CR degradation. Nevertheless, with the addition of EDTA and KI as scavengers, the degradation was dramatically suppressed for the three compounds. Of note, a similar desorption uptrend was observed for degradation of the three dyes once EDTA was dosed after 5 min adsorption, which might be attributed to the depletion of the active adsorption sites by the competition effect of EDTA. Hence, it can be deduced that the degradation of RhB, MB, and CR under visible light primarily proceeded by h^+, e^-, and $^{\bullet}O_2^-$, rather than $^{\bullet}OH$ or $^1O_2$ [56,57].

Based on the above results and analysis, the degradation mechanism of the selected dyes by $BiOI_{0.5}Cl_{0.5}$ under visible light irradiation is illustrated in Fig. 16. Under visible light irradiation, the dyes adsorbed on the catalyst are regarded as sensitizers and stimulated to generate electrons (e^-) that subsequently transfer to the recombination of the electrons and holes, and several ROS are produced and react with the organics. The electrons in the CB of $BiOI_{0.5}Cl_{0.5}$ can reduce the O_2 adsorbed on the surface of the $BiOI_{0.5}Cl_{0.5}$ nanorods to $^{\bullet}O_2^-$ through one electron reducing reaction [58]. The adsorbed molecular oxygen on the $BiOI_{0.5}Cl_{0.5}$ captures the electrons in the CB forming active $^{\bullet}O_2^-$, which acts as an oxidant. Normally, both $^{\bullet}O_2^-$ and h^+ can degrade the pollutants, and whether oxidation occurs indirectly by $^{\bullet}O_2^-$ or directly by h^+ appears to depend on the target substrates [27]. However, the photo-generated holes could also lead the generation of $^{\bullet}OH$ radicals due to the redox potential difference between Bi^{5+}/Bi^{3+} and $^{\bullet}OH/OH^-$ [59]. The oxidation potential of $BiOI_{0.5}Cl_{0.5}$ is 1.78 eV, which indicates that the holes cannot oxidize water molecules adsorbed on the surface of $BiOI_{0.5}Cl_{0.5}$ and generate $^{\bullet}OH$ (2.7 V) [58], deducing that $^{\bullet}OH$ is not a major active specie in our coupled system.

Based on the photodegradation performance of the three dyes, the mechanism is summarized in the following equations (Eqs. (9)–(12)) [60].

$$BiOI_{0.5}Cl_{0.5} + hv \rightarrow BiOI_{0.5}Cl_{0.5}\left(e^- + h^+\right) \quad (9)$$

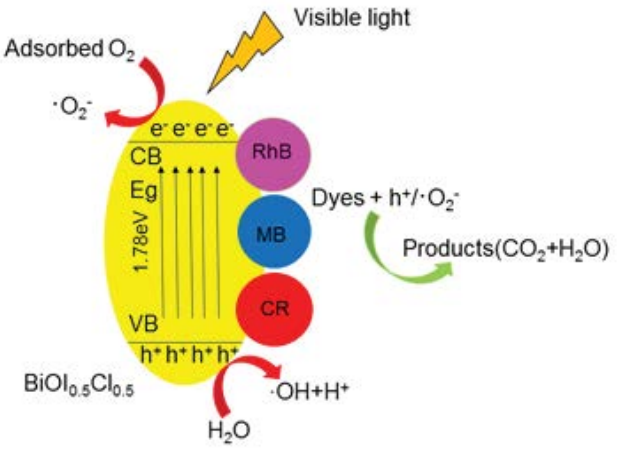

Fig. 16. Proposed mechanism for dyes degradation using $BiOI_{0.5}Cl_{0.5}$ under visible light irradiation.

$$BiOI_{0.5}Cl_{0.5}\left(e^-\right)+H_2O\rightarrow {}^{\bullet}OH+BiOI_{0.5}Cl_{0.5}+H^+ \quad (10)$$

$$BiOI_{0.5}Cl_{0.5}(e^-)+\text{adsorbed}\,O_2\rightarrow {}^{\bullet}O_2^-+BiOI_{0.5}Cl_{0.5} \quad (11)$$

$$\frac{\text{Adsorbed dye}+h^+}{{}^{\bullet}O_2^-\rightarrow \text{products}\rightarrow CO_2+H_2O} \quad (12)$$

4. Conclusions

The hierarchical nanoplate $BiOI_{0.5}Cl_{0.5}$ was successfully synthesized by a solvothermal method with narrow band gap of 1.78 eV, and high adsorption capacities for RhB, MB, and CR were obtained and fitted by pseudo-second-order kinetics and the Langmuir models. Compared to single adsorption, significant enhancement was achieved for the coupled process under visible light irradiation. Temperature showed limited effect on the adsorption, while an integrated impact was observed in various pH conditions especially for photocatalytic removals due to the characteristics of surface charge, deprotonation/protonation, and the reactive species. Increasing catalyst dosages exhibited promotion for the dye-degradation. By using the Langmuir–Hinshelwood (L–H) model, the kinetics concerning k_{app} were well-fitted and calculated under various conditions. The major reactive species were verified as h^+ and O_2^- through quenching studies with a degradation mechanism proposed for the coupled process. However, further studies are still needed to evaluate the mineralization and photochemical properties change for the residual metachromatic dyes in aquatic environments.

Acknowledgments

This work was financially supported by the National Natural Science Foundation of China (No. 51508354, 51878422), Science and Technology Projects of Sichuan Province (2018 HH0104), Science and Technology Bureau of Chengdu (2017-GH02–00010-HZ) and Innovation Spark Project in Sichuan University (2082604401254). The authors are thankful to all the anonymous reviewers for their insightful comments and suggestions.

References

[1] W. Huang, Y. Hu, Y. Li, Y. Zhou, D. Niu, Z. Lei, Z. Zhang, Citric acid-crosslinked β-cyclodextrin for simultaneous removal of bisphenol A, methylene blue and copper: the roles of cavity and surface functional groups, J. Taiwan Inst. Chem. Eng., 82 (2018) 189–197.
[2] U. Kamran, H.N. Bhatti, M. Iqbal, S. Jamil, M. Zahid, Biogenic synthesis, characterization and investigation of photocatalytic and antimicrobial activity of manganese nanoparticles synthesized from *Cinnamomum verum* bark extract, J. Mol. Struct., 1179 (2019) 532–539.
[3] R. Jiang, Y.Q. Fu, H.Y. Zhu, J. Yao, L. Xiao, Removal of methyl orange from aqueous solutions by magnetic maghemite/chitosan nanocomposite films: adsorption kinetics and equilibrium, J. Appl. Polym. Sci., 125 (2012) E540–E549.
[4] C. He, L. Shi, S. Lou, B. Liu, W. Zhang, L. Zhang, Synthesis of spherical magnetic calcium modified chitosan micro-particles with excellent adsorption performance for anionic-cationic dyes, Int. J. Biol. Macromol., 128 (2019) 593–602.
[5] J.A. Gonzalez, M.E. Villanueva, L.L. Piehl, G.J. Copello, Development of a chitin/graphene oxide hybrid composite for the removal of pollutant dyes: adsorption and desorption study, Chem. Eng. J., 280 (2015) 41–48.
[6] D. Morshedi, Z. Mohammadi, M.M.A. Boojar, F. Aliakbari, Using protein nanofibrils to remove azo dyes from aqueous solution by the coagulation process, Colloids Surf., B, 112 (2013) 245–254.
[7] A. Karunya, C. Rose, C.V. Nachiyar, Biodegradation of the textile dye Mordant Black 17 (calcon) by *Moraxella osloensis* isolated from textile effluent-contaminated site, World J. Microbiol. Biotechnol., 30 (2014) 915–924.
[8] Y.P. Zheng, G.H. Yao, Q.B. Cheng, S.C. Yu, M.H. Liu, C.J. Gao, Positively charged thin-film composite hollow fiber nanofiltration membrane for the removal of cationic dyes through submerged filtration, Desalination, 328 (2013) 42–50.
[9] L. Cheng, M.Y. Wei, L.H. Huang, F. Pan, D.S. Xia, X.X. Li, A.H. Xu, Efficient H_2O_2 oxidation of organic dyes catalyzed by simple copper(II) ions in bicarbonate aqueous solution, Ind. Eng. Chem. Res., 53 (2014) 3478–3485.
[10] X.R. Zhao, L.H. Zhu, Y.Y. Zhang, J.C. Yan, X.H. Lu, Y.P. Huang, H.Q. Tang, Removing organic contaminants with bifunctional iron modified rectorite as efficient adsorbent and visible light photo-Fenton catalyst, J. Hazard. Mater., 215 (2012) 57–64.
[11] E. Moctezuma, E. Leyva, C.A. Aguilar, R.A. Luna, C. Montalvo, Photocatalytic degradation of paracetamol: intermediates and total reaction mechanism, J. Hazard. Mater., 243 (2012) 130–138.
[12] O.F. Lopes, K.T.G. Carvalho, A.E. Nogueira, W. Avansi, C. Ribeiro, Controlled synthesis of $BiVO_4$ photocatalysts: evidence of the role of heterojunctions in their catalytic performance driven by visible-light, Appl. Catal., B, 188 (2016) 87–97.
[13] J.J. Zheng, Z.B. Jiao, Modified Bi_2WO_6 with metal-organic frameworks for enhanced photocatalytic activity under visible light, J. Colloid Interface Sci., 488 (2017) 234–239.
[14] L. Ren, S.Y. Lu, J.Z. Fang, Y. Wu, D.Z. Chen, L.Y. Huang, Y.F. Chen, C. Cheng, Y. Liang, Z.Q. Fang, Enhanced degradation of organic pollutants using $Bi_{25}FeO_{40}$ microcrystals as an efficient reusable heterogeneous photo-Fenton like catalyst, Catal. Today, 281 (2017) 656–661.
[15] J. Wang, H. Guo, Y. Liu, W. Li, B. Yang, Peroxymonosulfate activation by porous $BiFeO_3$ for the degradation of bisphenol AF: non-radical and radical mechanism, Appl. Surf. Sci., 507 (2020) 145097.
[16] L.Q. Ye, Y.R. Su, X.L. Jin, H.Q. Xie, C. Zhang, Recent advances in BiOX (X = Cl, Br and I) photocatalysts: synthesis, modification, facet effects and mechanisms, Environ. Sci. Nano, 1 (2014) 90–112.
[17] W.J. Kim, D. Pradhan, B.K. Min, Y. Sohn, Adsorption/photocatalytic activity and fundamental natures of BiOCl and $BiOCl_xI_{1-x}$ prepared in water and ethylene glycol environments, and Ag and Au-doping effects, Appl. Catal., B, 147 (2014) 711–725.

[18] H.J. Zhang, Y.X. Yang, Z. Zhou, Y.P. Zhao, L. Liu, Enhanced photocatalytic properties in BiOBr nanosheets with dominantly exposed (102) facets, J. Phys. Chem. C, 118 (2014) 14662–14669.
[19] L.M. Sun, L. Xiang, X. Zhao, C.J. Jia, J. Yang, Z. Jin, X.F. Cheng, W.L. Fan, Enhanced visible-light photocatalytic activity of BiOI/BiOCl heterojunctions: key role of crystal facet combination, ACS Catal., 5 (2015) 3540–3551.
[20] X.a. Dong, W. Zhang, Y. Sun, J. Li, W. Cen, Z. Cui, H. Huang, F. Dong, Visible-light-induced charge transfer pathway and photocatalysis mechanism on Bi semimetal@defective BiOBr hierarchical microspheres, J. Catal., 357 (2018) 41–50.
[21] X.F. Chang, M.A. Gondal, A.A. Al-Saadi, M.A. Ali, H.F. Shen, Q. Zhou, J. Zhang, M.P. Du, Y.S. Liu, G.B. Ji, Photodegradation of Rhodamine B over unexcited semiconductor compounds of BiOCl and BiOBr, J. Colloid Interface Sci., 377 (2012) 291–298.
[22] H. Li, L. Zhang, Photocatalytic performance of different exposed crystal facets of BiOCl, Curr. Opin. Green Sustainable Chem., 6 (2017) 48–56.
[23] J. Li, X.a. Dong, Y. Sun, W. Cen, F. Dong, Facet-dependent interfacial charge separation and transfer in plasmonic photocatalysts, Appl. Catal., B, 226 (2018) 269–277.
[24] X.Y. Qin, H.F. Cheng, W.J. Wang, B.B. Huang, X.Y. Zhang, Y. Dai, Three dimensional BiOX (X = Cl, Br and I) hierarchical architectures: facile ionic liquid-assisted solvothermal synthesis and photocatalysis towards organic dye degradation, Mater. Lett., 100 (2013) 285–288.
[25] X. Xiao, R. Hao, M. Liang, X.X. Zuo, J.M. Nan, L.S. Li, W.D. Zhang, One-pot solvothermal synthesis of three-dimensional (3D) BiOI/BiOCl composites with enhanced visible-light photocatalytic activities for the degradation of bisphenol-A, J. Hazard. Mater., 233 (2012) 122–130.
[26] H. Wang, W. Zhang, X. Li, J. Li, W. Cen, Q. Li, F. Dong, Highly enhanced visible light photocatalysis and in situ FT-IR studies on Bi metal@defective BiOCl hierarchical microspheres, Appl. Catal., B, 225 (2018) 218–227.
[27] X.N. Wang, W.L. Bi, P.P. Zhai, X.B. Wang, H.J. Li, G. Mailhot, W.B. Dong, Adsorption and photocatalytic degradation of pharmaceuticals by $BiOCl_xI_y$ nanospheres in aqueous solution, Appl. Surf. Sci., 360 (2016) 240–251.
[28] Y.Y. Zhang, X.G. Sun, G.Z. Yang, Y.H. Zhu, H.Y. Si, J.M. Zhang, Y.T. Li, Preparation and characterization of bifunctional $BiOCl_xI_y$ solid solutions with excellent adsorption and photocatalytic abilities for removal of organic dyes, Mater. Sci. Semicond. Process., 41 (2016) 193–199.
[29] C. Long, W. Ren, Y. Li, L. Liu, Y. Xia, H. Fan, High oxide ion conductivity in layer-structured $Bi_4Ti_3O_{12}$-based ferroelectric ceramics, J. Mater. Chem. C, 7 (2019) 8825–8835.
[30] P. Wang, Y.L. Wu, J. Shi, D. Liu, W.B. Dong, Preparation of carbon-supported Bi/Ti composites and its catalytic activity under solar irradiation, Appl. Surf. Sci., 292 (2014) 1077–1082.
[31] F. Dong, Y.J. Sun, M. Fu, Z.B. Wu, S.C. Lee, Room temperature synthesis and highly enhanced visible light photocatalytic activity of porous BiOI/BiOCl composites nanoplates microflowers, J. Hazard. Mater., 219 (2012) 26–34.
[32] Y.Q. Qu, X.F. Duan, Progress, challenge and perspective of heterogeneous photocatalysts, Chem. Soc. Rev., 42 (2013) 2568–2580.
[33] J.X. Xia, J. Di, H.T. Li, H. Xu, H.M. Li, S.J. Guo, Ionic liquid-induced strategy for carbon quantum dots/BiOX (X = Br, Cl) hybrid nanosheets with superior visible light-driven photocatalysis, Appl. Catal., B, 181 (2016) 260–269.
[34] J. Xie, Y.L. Cao, D.Z. Jia, H.Y. Qin, Z.T. Liang, Room-temperature solid-state synthesis of BiOCl hierarchical microspheres with nanoplates, Catal. Commun., 69 (2015) 34–38.
[35] V. Bernal, L. Giraldo, J.C. Moreno-Piraján, Insight into adsorbate–adsorbent interactions between aromatic pharmaceutical compounds and activated carbon: equilibrium isotherms and thermodynamic analysis, Adsorption, 26 (2020) 153–163.
[36] A.R. Bagheri, M. Ghaedi, Synthesis of chitosan based molecularly imprinted polymer for pipette-tip solid phase extraction of Rhodamine B from chili powder samples, Int. J. Biol. Macromol., 139 (2019) 40–48.
[37] T.A. Ojo, A.T. Ojedokun, O.S. Bello, Functionalization of powdered walnut shell with orthophosphoric acid for Congo red dye removal, Part. Sci. Technol., 37 (2017) 74–85.
[38] A. Pettignano, N. Tanchoux, T. Cacciaguerra, T. Vincent, L. Bernardi, E. Guibal, F. Quignard, Sodium and acidic alginate foams with hierarchical porosity: preparation, characterization and efficiency as a dye adsorbent, Carbohydr. Polym., 178 (2017) 78–85.
[39] M.Q. Yan, Q.W. Fu, D.C. Li, G.F. Gao, D.S. Wang, Study of the pH influence on the optical properties of dissolved organic matter using fluorescence excitation-emission matrix and parallel factor analysis, J. Lumin., 142 (2013) 103–109.
[40] J. Jiang, K. Zhao, X.Y. Xiao, L.Z. Zhang, Synthesis and facet-dependent photoreactivity of BiOCl single-crystalline nanosheets, J. Am. Chem. Soc., 134 (2012) 4473–4476.
[41] K.X. Ren, K. Zhang, J. Liu, H.D. Luo, Y.B. Huang, X.B. Yu, Controllable synthesis of hollow/flower-like BiOI microspheres and highly efficient adsorption and photocatalytic activity, CrystEngComm, 14 (2012) 4384–4390.
[42] K. Natarajan, H.C. Bajaj, R.J. Tayade, Photocatalytic efficiency of bismuth oxyhalide (Br, Cl and I) nanoplates for RhB dye degradation under LED irradiation, J. Ind. Eng. Chem., 34 (2016) 146–156.
[43] A. Salama, Preparation of CMC-g-P(SPMA) super adsorbent hydrogels: exploring their capacity for MB removal from waste water, Int. J. Biol. Macromol., 106 (2018) 940–946.
[44] H.G. Guo, T.L. Ke, N.Y. Gao, Y. Liu, X. Cheng, Enhanced degradation of aqueous norfloxacin and enrofloxacin by UV-activated persulfate: kinetics, pathways and deactivation, Chem. Eng. J., 316 (2017) 471–480.
[45] Y.W. Gao, Y. Wang, H. Zhang, Removal of Rhodamine B with Fe-supported bentonite as heterogeneous photo-Fenton catalyst under visible irradiation, Appl. Catal., B, 178 (2015) 29–36.
[46] T.Y. Xu, R.L. Zhu, G.Q. Zhu, J.X. Zhu, X.L. Liang, Y.P. Zhu, H.P. He, Mechanisms for the enhanced photo-Fenton activity of ferrihydrite modified with $BiVO_4$ at neutral pH, Appl. Catal., B, 212 (2017) 50–58.
[47] S.K. Maeng, K. Cho, B. Jeong, J. Lee, Y. Lee, C. Lee, K.J. Choi, S.W. Hong, Substrate-immobilized electrospun TiO_2 nanofibers for photocatalytic degradation of pharmaceuticals: the effects of pH and dissolved organic matter characteristics, Water Res., 86 (2015) 25–34.
[48] A. Takdastan, B. Kakavandi, M. Azizi, M. Golshan, Efficient activation of peroxymonosulfate by using ferroferric oxide supported on carbon/UV/US system: a new approach into catalytic degradation of bisphenol A, Chem. Eng. J., 331 (2018) 729–743.
[49] N.G. Asenjo, R. Santamaria, C. Blanco, M. Granda, P. Alvarez, R. Menendez, Correct use of the Langmuir–Hinshelwood equation for proving the absence of a synergy effect in the photocatalytic degradation of phenol on a suspended mixture of titania and activated carbon, Carbon, 55 (2013) 62–69.
[50] M.L. Li, G.F. Chen, Revisiting catalytic model reaction p-nitrophenol/$NaBH_4$ using metallic nanoparticles coated on polymeric spheres, Nanoscale, 5 (2013) 11919–11927.
[51] L.J. Xu, J.L. Wang, Magnetic nanoscaled Fe_3O_4/CeO_2 composite as an efficient Fenton-like heterogeneous catalyst for degradation of 4-chlorophenol, Environ. Sci. Technol., 46 (2012) 10145–10153.
[52] Z.F. Huang, H.W. Bao, Y.Y. Yao, W.Y. Lu, W.X. Chen, Novel green activation processes and mechanism of peroxymonosulfate based on supported cobalt phthalocyanine catalyst, Appl. Catal., B, 154 (2014) 36–43.
[53] X.B. Wang, Y.L. Qin, L.H. Zhu, H.Q. Tang, Nitrogen-doped reduced graphene oxide as a bifunctional material for removing bisphenols: synergistic effect between adsorption and catalysis, Environ. Sci. Technol., 49 (2015) 6855–6864.
[54] J. Jia, P. Xue, R. Wang, X. Bai, X. Hu, J. Fan, E. Liu, The Bi/Bi_2WO_6 heterojunction with stable interface contact and enhanced visible-light photocatalytic activity for phenol and Cr(VI) removal, J. Chem. Technol. Biotechnol., 93 (2018) 2988–2999.

[55] Y. Liu, H. Guo, Y. Zhang, X. Cheng, P. Zhou, J. Wang, W. Li, Fe@C carbonized resin for peroxymonosulfate activation and bisphenol S degradation, Environ. Pollut., 252 (2019) 1042–1050.
[56] H. Gnayem, Y. Sasson, Nanostructured 3D sunflower-like bismuth doped $BiOCl_xBr_{1-x}$ solid solutions with enhanced visible light photocatalytic activity as a remarkably efficient technology for water purification, J. Phys. Chem. C, 119 (2015) 19201–19209.
[57] A. Kausar, G. MacKinnon, A. Alharthi, J. Hargreaves, H.N. Bhatti, M. Iqbal, A green approach for the removal of Sr(II) from aqueous media: kinetics, isotherms and thermodynamic studies, J. Mol. Liq., 257 (2018) 164–172.
[58] Y. Peng, K.K. Wang, T. Liu, J. Xu, B.G. Xu, Synthesis of one-dimensional Bi_2O_3-$Bi_2O_{2.33}$ heterojunctions with high interface quality for enhanced visible light photocatalysis in degradation of high-concentration phenol and MO dyes, Appl. Catal., B, 203 (2017) 946–954.
[59] S. Gao, C. Guo, J. Lv., A novel 3D hollow magnetic Fe_3O_4/BiOI heterojunction with enhanced photocatalytic performance for bisphenol A degradation, Chem. Eng. J., 307 (2017)1055–1065.
[60] B. Subash, B. Krishnakumar, M. Swaminathan, M. Shanthi, Highly efficient, solar active, and reusable photocatalyst: Zr-loaded Ag-ZnO for Reactive Red 120 dye degradation with synergistic effect and dye-sensitized mechanism, Langmuir, 29 (2013) 939–949.